doi:10.1006/jmbi.2000.3885 available online at http://www.idealibrary.com on IDEAL® J. Mol. Biol. (2000) 300, 677–685

JMB

COMMUNICATION

Use of a New Label, $^{13}C{=}^{18}O$, in the Determination of a Structural Model of Phospholamban in a Lipid Bilayer. Spatial Restraints Resolve the Ambiguity Arising from Interpretations of Mutagenesis Data

Jaume Torres[1], Paul D. Adams[2] and Isaiah T. Arkin[1]*

[1]*Cambridge Centre for Molecular Recognition Department of Biochemistry University of Cambridge, 80 Tennis Court Road, Cambridge CB2 1GA, UK*

[2]*Lawrence Berkeley National Laboratory, 1 Cyclotron Road Berkeley, California CA 94720, USA*

**Corresponding author*

A structural model of pentameric phospholamban (Plb) in a lipid bilayer has been derived using a combination of experimental data, obtained from ATR-FTIR site-directed dichroism, and the implementation of the resulting restraints during a molecular dynamics simulation. Plb (residues 24-52) has been synthesised incorporating a new label, 1-$^{13}C{=}^{18}O$, at residues 42 and 43. We have not only determined the tilt of the helices, 10(±6)°, but also the relative orientation of the transmembrane segments, with an ω angle of −32(±10)° for L42. This angle is taken as zero in the direction of the helix tilt. Plb is a simple test case where site-directed dichroism has been applied to resolve the indeterminacy arising from the mutagenesis data available. The results presented point specifically to a single structural model for Plb.

Keywords: phospholamban; ion channel; infrared spectroscopy; molecular dynamics

Introduction

Phospholamban (Plb) is a 52-residue protein located in the cardiac sarcoplasmic reticulum. Plb contains a hydrophilic, mostly helical domain in the cytosol (residues 1-25), and a hydrophobic domain (residues 26-52) that forms a transmembrane α-helix (see Arkin *et al*., 1997; Simmerman & Jones, 1998) for recent reviews. Plb can be found in different states of aggregation, although preferentially it polymerises as a pentamer (Wegener & Jones, 1984). The recognised function of Plb is to act as an inhibitor of Ca^{+2}ATPase (Kirchberger & Tada, 1976). This inhibition is thought to be caused by the binding of the monomeric form of Plb to the Ca^{+2}ATPase (Autry & Jones, 1997; Kimura *et al*., 1996), although other studies (Toyofuku *et al*., 1994; Kimura *et al*., 1998; Chu *et al*., 1997, 1998) have shown that the oligomeric assembly could be also important for Ca^{+2} ATPase regulation. Inhibition of the Ca^{+2}ATPase is removed upon Plb phosphorylation, which has been suggested to induce pentamerisation in lipid bilayers but not in SDS, based on results from electron paramagnetic resonance (Cornea *et al*., 1997). It is the ability to form pentamers, and the deleterious effects of Plb when expressed in heterologous systems, that have led to the suggestion that Plb could act also as an ion channel (Kovacs *et al*., 1988; Cook *et al*., 1989).

The structure of Plb has been the subject of a number of studies, mainly based on mutagenesis data (Fujii *et al*., 1989; Arkin *et al*., 1994; Simmerman *et al*., 1996; Kimura *et al*., 1997). The wealth of information concerning the residues that are important in maintaining the pentameric structure has led to a consensus regarding the general arrangement of the transmembrane helical segments. The resulting pattern of sensitivity towards substitution, analysed by helical wheel diagrams, was found to be compatible with a left-handed coiled coil (i.e. 3.5 residues per turn) (Arkin *et al*., 1994). Furthermore, the periodical occurrence of Leu and Ile residues in the Plb sequence led to the suggestion that the motif that provides stability to the pentamer is analogous to a leucine zipper (Simmerman *et al*., 1996). This model however, contrasts with a model presented by Adams *et al*. (1995), which is also consistent with the mutagenesis data, in which the helices are rotated ~45° around their longitudinal axes respect to the latter model.

E-mail address of the corresponding author: sa232@cam.ac.uk

0022-2836/00/040677–9 $35.00/0

More recently, labelling experiments performed in SDS have been reported (Karim *et al*., 1998) that strongly support the leucine-zipper model. Also, in a purely theoretical work (Herzyk & Hubbard, 1998), restraints based on the mutagenesis data were introduced as a sole guiding force in a Monte-Carlo simulated annealing protocol. The two models referred to above were obtained and, assuming a different interpretation of the mutagenesis data, the model presented by Simmerman *et al*. (1996) (i.e. the so-called leucine zipper) was preferred.

Here, which has proved to be more useful and conclusive than mutagenesis or labelling studies, we have determined experimentally the oligomerisation model of Plb in a system that is more suitable than SDS, a hydrated lipid bilayer. We have used spatial restraints derived from the infrared dichroisms of the peptidic $^{12}C{=}O$ bonds (helix) and from the introduced $^{13}C{=}^{18}O$ bonds (labels) present at specific sites. This label produces a band that is completely shifted from the amide I (Torres *et al*., unpublished results), allowing the determination of its area without the need for deconvolution.

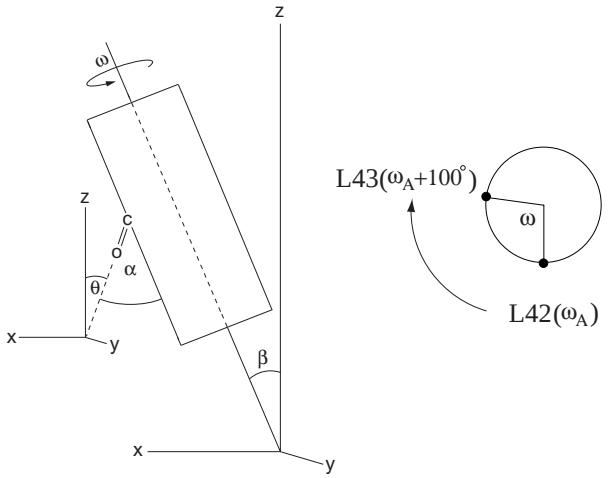

Figure 1. Left: schematic of the geometric parameters that define the amide I (C═O) transition dipole moment orientation in a transmembrane helix. The helix tilt β and the rotational orientation ω are derived from the experimental data. The angle α is 39° (Tsuboi, 1962) and θ is obtained from β, α and ω and is used as a restraint (see the text). Right: schematic vertical view for the relative positions of labels L42 and L43 showing their distribution around the helical axis. The helical segment has been drawn as a perfect cylinder for simplicity.

Materials and methods

Peptide purification and reconstitution

The transmembrane segment of Plb (residues 25 to 52) was synthesised by standard solid-phase F-moc chemistry, cleaved from the resin with trifluoroacetic acid (TFA) and lyophilised. During the synthesis of the peptide, two labelled residues with a $^{13}C{=}^{18}O$ carbonyl were introduced at positions L42 or L43, as seen in Figure 1. The two oxygen atoms in the carboxylic group of leucine labelled with $^{13}C{=}^{16}O$ (Cambridge Isotopes Laboratories, Andover, MA) were exchanged to ^{18}O (Torres *et al*., unpublished results) incubating the amino acid at 100 °C at acidic pH conditions (approximately 1) with a mixture of $H_2{}^{18}O$ and dioxane (3:1 (v/v)) for one hour. The extent of exchange was obtained using mass spectrometry. About 50 % of the residue was completely exchanged (with two oxygen atoms) and the other half was only partially exchanged (one oxygen atom). Therefore, approximately 75 % of the molecules of peptide in the sample should have a $^{13}C{=}^{18}O$-labelled residue. Needless to say however, this percentage is totally irrelevant, as the determination of the dichroism of the label, provided it can be measured, is completely independent from its relative abundance in the sample.

The mixture was lyophilised and the amino acid was derivatised with FMOC as described (Wellings & Atherton, 1997). The lyophilised peptides were dissolved in 2 ml of formic acid (final concentration, ca 5 mg/ml) and immediately injected onto a 20 ml Jupiter5 C4-300 Å column (Phenomenex, Cheshire, UK) connected to an HPLC system (Biocad Sprint, Perceptive Biosystems, Cambridge, USA). The solvents used were: solvent A, water:-TFA (99.9:0.1 (v/v)); solvent B, isopropanol:acetonitrile:water:TFA (38:57:5:0.1 (v/v/v/v)) and solvent C, trifluoroethanol:water:TFA (95:5:0.1 (v/v/v)).

The column was previously equilibrated with a mixture of solvents A and B (9:1). After a linear increase to 100 % in B, the concentration of C was increased linearly to 35 % and the peptide was eluted. Pooled fractions were lyophilised and the purity of the samples was checked by mass spectrometry, which did not show the presence of adducts (adducts were observed if the peptide was dissolved in TFA instead of formic acid). The lyophilised peptide was dissolved in a solution containing 5 % (w/v) β-octylglycopyranoside (Sigma, St. Louis, USA) and 12.5 mg/ml dimyristoylphosphocholine (DMPC) (Sigma, St. Louis, USA). The samples were dialysed (Spectra/Por 4 cut-off 12-14,000 d, Spectrum Laboratories, Laguna Hills, CA, USA) for two days against water and a further 12 hours against 0.1 mM phosphate $K_2HPO_4{\cdot}K_2PO_4$ buffer (pH~7.0). After the dialysis, the samples were concentrated by centrifugation at ~90,000 ***g*** for 30 minutes in a Beckman 50Ti rotor (Beckman Coulter, Inc., Fullerton, CA, USA) and resuspended.

Infrared spectroscopy

FTIR spectra were recorded on a Nicolet Magna 560 spectrometer (Madison, USA) purged with N_2 and equipped with a MCT/A detector cooled with

liquid nitrogen. Attenuated total reflection (ATR) spectra were measured with a 25-reflections ATR accessory from Graseby Specac (Kent, UK) and a wire grid polariser (0.25 μM, Graseby Specac). Approximately 200 μl of sample (~2.5 mg/ml protein and 12.5 mg/ml lipid) were applied onto a trapezoidal (50 mm × 2 mm × 20 mm) internal reflection element (KRS-5 or Ge) and bulk water was removed using a dry N_2 stream. After insertion of the plate in the ATR cell, spectra were collected. Other spectra were collected after flushing the interior of the ATR cell with nitrogen that was bubbled through two compartments containing either ^2H_2O or H_2O for 48 hours. A total of 1000 interferograms collected at a resolution of 4 cm^{-1} were averaged for every sample and processed with one-point zero filling and Happ-Genzel apodisation.

The area corresponding to the $^{13}C{=}{=}^{18}O$ (isotope-labelled) carbonyl stretching vibration was obtained integrating the band at 1590 cm^{-1}. The area of the amide I (corresponding to helical structure) was obtained by peak integration from 1670 to 1645 cm^{-1}. No difference in the band intensity was observed employing other means of peak size estimation such as peak fitting and Fourier self-deconvolution.

The analysis of the hydrated spectra was performed in a more elaborated way. First, because H_2O absorbs in the amide I region and it is not possible to obtain an accurate dichroism for the helix. Second, because the bending O-^{2}H vibration of ^2H_2O interferes with the absorbance of the label at 1590 cm^{-1} (not shown). This was overcome by using the ^2H_2O-hydrated sample to calculate the helix dichroism and the H_2O-hydrated sample to calculate the label dichroism. As there is some interference of the H_2O band at 1590 cm^{-1}, the dichroism of the label was obtained after subtracting a spectrum of hydrated lipid (in H_2O) from the spectrum of the sample hydrated in H_2O. Only the dichroism of the site was obtained in this case, as is much less affected by the water band than the amide I. The helix dichroism was measured from the amide I spectrum or the amide A (N-H stretching, centred at ~3300 cm^{-1}) when the sample was hydrated in ^2H_2O. The dichroic ratio was calculated as the ratio between the integrated absorptions of the spectra collected with parallel and perpendicular polarised light.

Data analysis

The data was analysed according to the theory of site-specific dichroism (Arkin *et al*., 1997). This technique is based on the fact that the measured dichroism, $\mathcal{R}$ of a particular transition dipole moment is a function of the sample fractional order, f and the spatial orientation of the dipole, which is defined by the parameters shown in Figure 1: β, the helix-tilt, α, which relates the transition dipole moment to the helix director and ω, the rotational pitch angle. The rotational pitch angle ω is arbitrarily defined as 0° when the C═O transition dipole moment, the helix director and the z-axis all reside in the same plane. The angle α is known from fibre diffraction studies, and is 39° for transition dipole moment of the peptidic C═O bond and 29° for the N-H bond (Tsuboi, 1962). It is noted that the precise values for the α angle have been debated for some time in the literature, but it is now generally agreed that the earlier reported values of below 30° were a result of a different configuration between the amide I mode and the peptidic plane. Furthermore, using site-directed dichroism in which three labels were employed, it was possible to confirm the value of the α angle for the amide I mode (Arkin *et al*., 1997).

From each measurement, two different dichroisms are obtained. The first is $\mathcal{R}_{\mathrm{Helix}_i}$, the dichroism that corresponds to the $^{12}C{=}O$ dipoles, or N-H in the case of amide A, involved in the helical structure. We note that when the dichroic ratio of the helix is obtained from the amide A dichroism, the dichroic ratio should reflect more accurately the tilt of the transmembrane domain. In fact, the amide A band in these conditions, i.e. the sample being exposed to ^2H_2O, originates only from the transmembrane α-helix that has not exchanged. This dichroism arises from residues distributed around the helical axis, (i.e. one every 100° for a standard α-helix). Therefore, this dichroism is independent of ω, and dependent only on β and f_i:

$$\mathcal{R}_{\mathrm{Helix}_i}(\beta,\, f_i) = \frac{e_z^2\left(f_i\mathcal{K}_z + \frac{1-f_i}{3}\right) + e_x^2\left(f_i\mathcal{K}_x + \frac{1-f_i}{3}\right)}{e_y^2\left(f_i\mathcal{K}_y + \frac{1-f_i}{3}\right)} \tag{1}$$

where $\mathcal{K}_{x,\ y\ \mathrm{or}\ z}(\langle\omega\rangle)$ are the rotationally averaged integrated absorption coefficients, f_i represents the fractional order of preparation i. The parameter f is 1 if the sample is completely ordered and zero if completely random. Finally, e_x, e_y and e_z are the electric field components for each axis given by Harrick (1967) according to a thick film approximation. The thickness of the film was calculated as being more than 30 μm, whereas the the amplitude of the evanescent wave decays (at $1/e$ of its initial value) after 1 μm in a germanium plate and about 7 μm in a KRS-5 plate.

The second dichroism, $\mathcal{R}_{Site_i}$, corresponds to the $^{13}C{=}{=}^{18}O$ i label, consequently it will be dependent on the ω angle for this particular label:

$$\mathcal{R}_{\mathrm{Sites}_i}(\beta,\, f_i,\, \omega) = \frac{e_z^2\left(f_i\mathcal{K}_z(\omega) + \frac{1-f_i}{3}\right) + e_x^2\left(f_i\mathcal{K}_x(\omega) + \frac{1-f_i}{3}\right)}{e_y^2\left(f_i\mathcal{K}_y(\omega) + \frac{1-f_i}{3}\right)} \tag{2}$$

These two equations are not sufficient to obtain β, ω and f_i (three unknowns), therefore a second label is inserted with a different ω. For example, if the label is inserted one residue above or below the first label (for a canonical α-helix there are 3.6 residues per turn) the increment in ω is 100°. Thus, two additional equations can be obtained. One is $\mathcal{R}_{\mathrm{Helix}_j}$, dependent on β and f_j and the other is $\mathcal{R}_{\mathrm{Site}_j}$, dependent on β, ω + 100° and f_j (Arkin *et al*., 1997). Solving these four equations for each i and j pair, will yield β_{ij}, ω_{ij}, f_i and f_j, where β_{ij} and ω_{ij} are the results obtained from the combinations of sample i and sample j (Kukol *et al*., 1999).

The non-linear equations were solved with Newton's method as implemented in the Find Root function in Mathematica 3.0 (Wolfram Research, Champaign, USA). The final values of β and ω were obtained by averaging β_{ij} and ω_{ij}, respectively:

$$\beta = \frac{1}{n^2}\sum_{i=1}^{n}\sum_{j=1}^{n}\beta_{ij}$$

$$\omega = \frac{1}{n^2}\sum_{i=1}^{n}\sum_{j=1}^{n}\omega_{ij} \qquad (3)$$

Note that the maximum dichroism $\mathcal{R}_{\max}$ for C═O groups in an α-helix was obtained from equation (1) ($\beta = 0, f = 1, \alpha = 39°$) and is 5.21 for KRS-5 and 4.34 for Ge.

Use of mutagenesis data

A qualitative estimation of the relative interaction energy per residue was calculated from the data published by Jones and co-workers (Simmerman *et al*., 1996). These results, although very similar to those published by Arkin *et al*. (1994), extend to residue 31 (35 in the latter), and are suited for a numerical adaptation, because residues were substituted only by either of two residues (Ala or Phe) and a percentage of pentamerisation relative to a control is estimated in each case.

Assuming that a higher level of sensitivity to mutation should indicate a higher level of interaction energy, we have calculated the numerical value assigned to each residue from these percentages of pentamerisation. For each residue, the percentage of pentamerisation following substitution by Ala (Simmerman *et al*., 1996) and Phe were weighted differently (0.8 and 0.2, respectively) to account for the different relevance of a failed pentamerisation in each case. This weighting of parameters are somewhat arbitrary but reflects the fact that the relevance of a failed pentamerisation is far greater when the residue is substituted by the relatively small and α-helix inducer Ala than by the bulkier Phe. This then was normalised to fit in a scale from 0 to 10, where 0 indicates no sensitivity to mutation (not even substitution by Ala disrupts the pentamer). This estimation was compared to the interaction energy per residue for each cluster using a χ^2 analysis given by:

$$\chi^2 = \frac{1}{n}\sum_{i}^{n}\frac{(o_i - m_i)^2}{m_i}$$

whereby o_i is the normalised interaction energy of residue i, and m_i is the normalised sensitivity to mutation of residue i calculated as described above.

Molecular modelling

A global search, in which the helices were rotated about their helical axis, was carried out as described (Adams *et al*., 1995) with some modifications (see below) and assuming a homo-pentameric conformation. All calculations were performed with PCNS, the parallel-processing version of the Crystallography and NMR System (CNS Version 0.3) (Brünger *et al*., 1998). The OPLS parameter set with united atom topology was used, representing explicitly polar hydrogens and aromatic side-chain atoms (Jorgensen & Tirado-Rives, 1988). All calculations were carried out *in vacuo* with the initial coordinates of a canonical α-helix (3.6 residues per turn). Symmetric pentamers were generated by duplicating and rotating the helix 72°.

An initial crossing angle of 25° for left handed and −25° for right-handed structures was introduced by rotating the long helix axis with respect to the long bundle axis. The symmetric pentamer search was carried out by rotating all the helices simultaneously between $\phi = 0°$ and $\phi = 360°$ in 10° steps. For each starting conformation, four trials were carried out at left and right-handed crossing angles, using different initial random velocities in each trial. This procedure results in a total of 288 different trials (i.e. $36 \times 4 \times 2$), which in turn produce 288 final structures. Each structure was subjected to a simulated annealing and an energy-minimisation protocol, as described (Adams *et al*., 1995).

The resulting structures were grouped in clusters, defined by having more than ten structures, and where every structure pertaining to a cluster was within 1.0 Å, RMSD from any other structure of the same cluster. The structures pertaining to the same cluster were averaged and this averaged structure was subjected to a simulated annealing protocol identical to that used in the systematic search and taken as representative of each cluster.

Two types of experimental restraints, obtained from site-directed infrared dichroism, were implemented in this search. First, the angle between the vectors connecting every C^α of residue i and C^α of residue $i + 7$ and the z-axis was restrained to β, the experimental value obtained for the helix tilt. Second, the angle between the cor-

responding $^{13}C{=}^{18}O$ bond and the *z*-axis were restrained to those obtained from the analysis (Arkin *et al*., 1997), see Figure 1. The application of these restraints resulted in a torque about the helix axis. This restraints are represented by the energy term:

$$E = k_{\text{dichro}}(\theta - \theta_0)^2 \quad (4)$$

where θ represents the current angle and θ_0 represents the target angle. The overall weight for these orientational constraints k_{dichro} was chosen to be 800 cal/grad^2, a value determined empirically (Kukol *et al*., 1999).

Results and Discussion

FTIR measurements

The spectra obtained after removing the bulk water from the samples or after hydrating the samples with a stream of ^2H_2O or H_2O-saturated N_2 for 48 hours are shown in Figure 2. In the first case, as shown in this Figure (a), a substantial amount of water is still present in the sample, as seen from the band at 3300 cm^{-1}.

The amide I region of Figure 2(a) for samples where L42 or L43 were labelled are shown in Figure 3. The intensity of the $\perp$ spectrum (right axis) has been normalised to that of the $\parallel$ spectrum (left axis).

The spectra, obtained with parallel ($\parallel$) or perpendicularly ($\perp$) polarised light are typical for a predominantly α-helical peptide (Byler & Susi, 1986), having an amide I band with maximum at 1657 cm^{-1}. Neither the original nor the deconvoluted (not shown) spectra show significant intensity around 1640-1630 cm^{-1}, indicating the absence of β structure (Byler & Susi, 1986). They show however, some intensity around 1680 cm^{-1}, suggesting the presence of some β-turns (Byler & Susi, 1986), probably located in the small extramembraneous part of the peptide.

The stretching vibration of the C═O bonds that contain a $^{13}C{=}^{18}O$ label produces a band at 1590 cm^{-1} which is not present in the spectrum of Plb labelled with $^{13}C{=}^{16}O$ (see Figure 4). Further, the position of this band is in agreement with recent theoretical calculations (Torres *et al*., unpublished results).

As two labels with different ω (L42 and L43) were used, we obtained, as described in Materials and Methods, two equations for each label. One corresponding to the dichroism of helix and the other to the dichroism of the label, giving a total of four equations. When this system of four equations was solved for the 30 combinations of measurements corresponding to samples L42 and L43 (i.e. 5×6), it became apparent that, even when using the combined data from samples where bulk water was removed and samples hydrated in ^2H_2O or H_2O, the results converge to a narrow range of ω angles, as shown in the bottom panel of Figure 5.

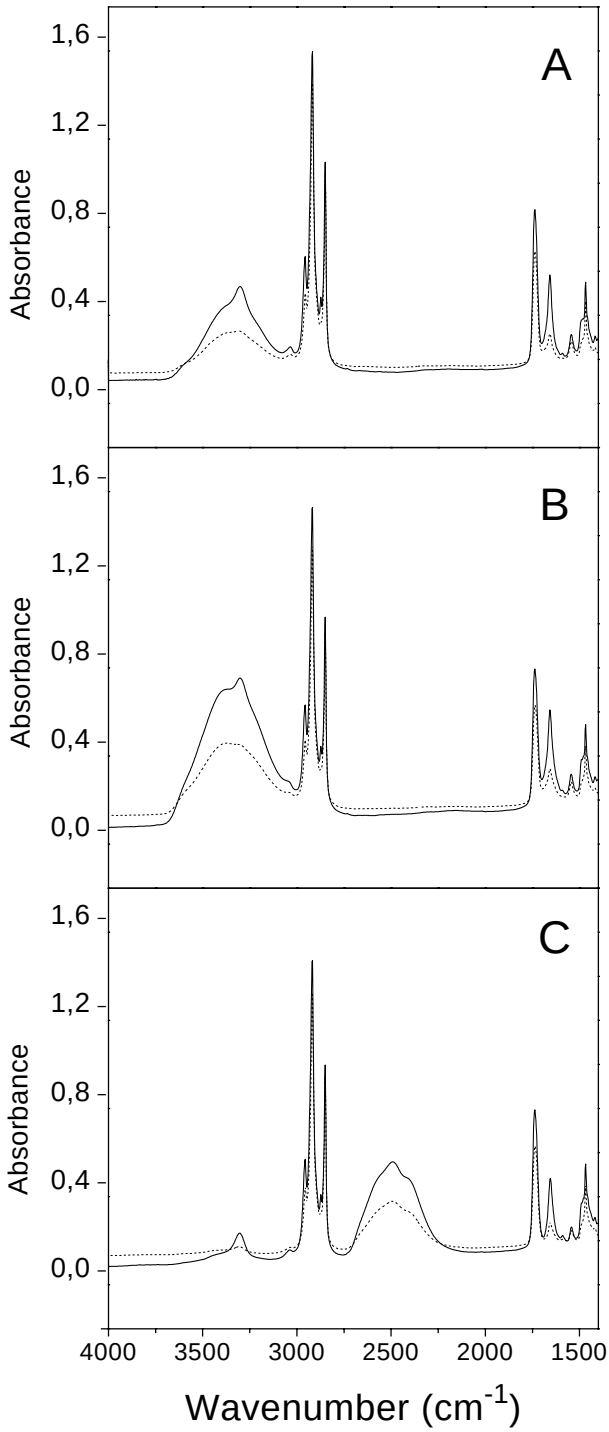

Figure 2. Spectra obtained with parallel (continuous line) and perpendicular (broken line) polarisation of spectra of phospholamban after removing bulk water with a stream of dry nitrogen (a), and after complete hydration (see Materials and Methods) with ^2H_2O (b) or H_2O (c).

The average ω_A was $-32(\pm 10)^\circ$, and the helix tilt β was $10(\pm 5)^\circ$.

The fractional order parameter was always around 0.5. The angle between the C═O bond of

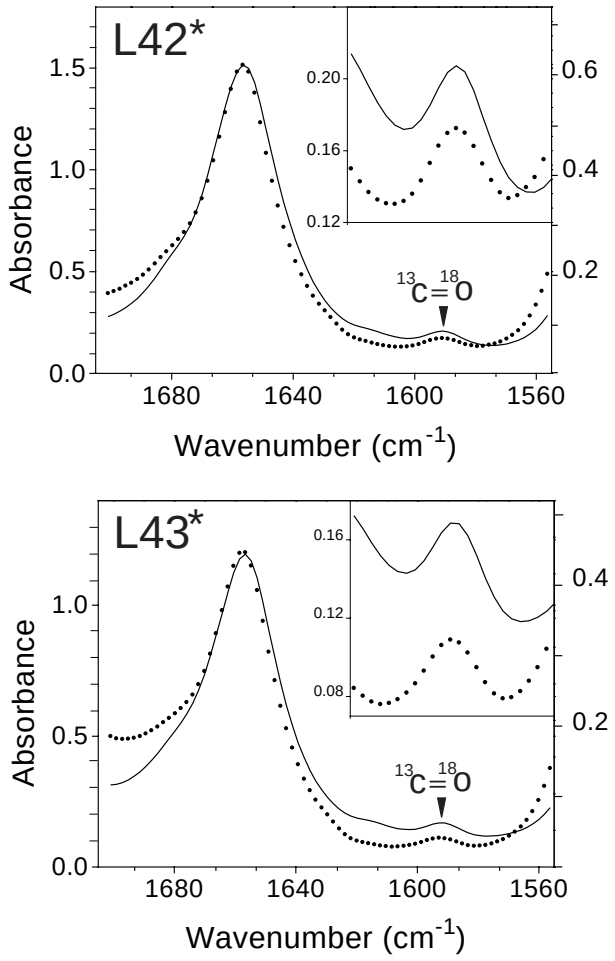

Figure 3. ATR-FTIR spectra corresponding to the original amide I region of the transmembrane domain of Plb obtained with parallel (continuous line) or perpendicular (broken line) polarised light. The residue labelled is indicated at the top left hand corner. The intensity of the $^{12}C{=}^{16}O$ band has been normalised for ($\perp$) and ($\parallel$) polarisation. The left and right axis indicate the absorbance of the spectra obtained using ($\parallel$) and ($\perp$) polarisation, respectively. The position of the band arising from the $^{13}C{=}^{18}O$ label is indicated. The inserts show the bands corresponding to the 1-$^{13}C{=}^{18}O$ label, centred at 1590 cm^{-1} using the same axes.

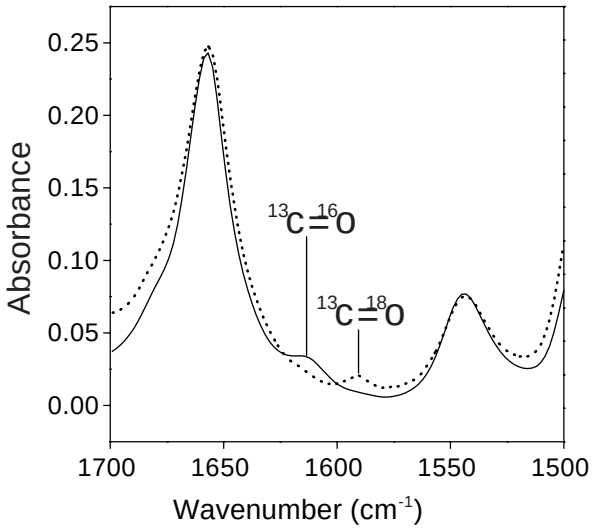

Figure 4. Amide I and II regions obtained with light polarised in parallel corresponding to a sample of Plb labelled at a single residue (L42) with $^{13}C{=}^{16}O$ (continuous line) and with $^{13}C{=}^{18}O$ (broken line).

the labels and the z-axis was found to be $\theta_{L42} = 17^\circ$ and $\theta_{L43} = 21^\circ$.

Modelling

These results were used as experimental restraints in molecular dynamics simulations as described in Materials and Methods. In particular, the angle between the vectors connecting every C^α of residue i and C^α of residue $i+7$ and the z-axis was restrained to 10°, i.e. the experimental value obtained for the helix tilt β. Also, the angles between the corresponding $^{13}C{=}^{18}O$ bonds and the z-axis, were restrained to 17° and 21°, which are the experimental values θ in sites L42 and L43 respectively, see Figure 1.

It is clear from the bottom panel in Figure 5 that cluster number 5 has the lowest energy. Also, the distribution of interaction energies per residue in clusters 5 and 6 are the most consistent with the mutagenesis data (see Materials and Methods), having the smallest χ^2 value (see horizontal bars in lower panel (Figure 5). Thus, taking only mutagenesis into account, these two models are indistinguishable. The calculated ω angle for residue L42 corresponding to cluster 5, however, (-32°) is entirely consistent with the value obtained experimentally for residue 42 (see grey area at lower panel). Therefore, these results allow us to discriminate between two different models suggested on the basis of mutagenesis experiments (Adams *et al.*, 1995) and (Simmerman *et al.*, 1996). Two slices, one for each of these two models are represented at the top of Figure 5. One model (Simmerman *et al.*, 1996) is similar to cluster 5 and the other (Adams *et al.*, 1995) is analogous to cluster 6. The residues corresponding to these slices have been coloured according to their sensitivity to mutation.

The leucine zipper-like arrangement (analogous to cluster 5) has found additional support in recent labelling experiments performed in SDS. In fact, evidence has been presented (Karim *et al.*, 1998) that cysteine 41 is the only cysteine labelled with DTNB when Plb forms a pentamer in SDS. This, assuming that the structure in SDS and in a lipid bilayer is the same, points to a structure analogous to cluster 5. Our results provide reliable and direct structural data that indicates that the structure of Plb in a lipid bilayer is represented by cluster 5, i.e.

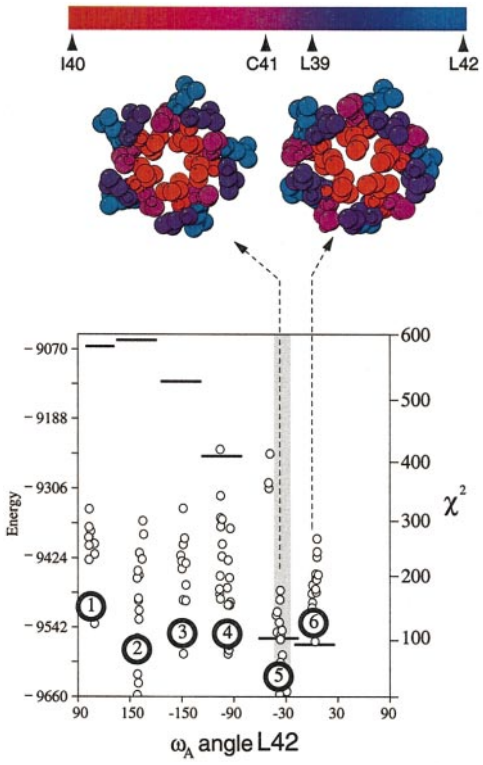

Figure 5. Results obtained using the restraints from site-directed dichroism. Top: slices of the Plb pentamer (residues 39-42) for the two configurations that are in agreement with the mutagenesis data. The atoms for each residue are coloured according to their involvement in the stability of the pentamer, in a scale from red (sensitive) to blue (non-sensitive), obtained as described in Materials and Methods. Bottom: result of the molecular dynamics simulation. The individual structures (small circles) that pertain to clusters are represented as a function of their energy and ω_{L42}. The average for each cluster is indicated by large circles with the corresponding cluster number inside. The degree of similarity between the calculated interaction energy for each of these average structures and the results from mutagenesis data was estimated by calculating a χ^2 value for every cluster (short horizontal lines). The scale for χ^2 is on the right axis. The two dotted arrows indicate the equivalence between clusters 5 and 6 and the two structures represented above. The grey rectangle is centred at $\omega_A - 32^\circ$ and its width corresponds to two standard deviations.

a structure analogous to that suggested by Simmerman *et al*. (1996).

This results however, are in contrast with previous H/^{2}H exchange experiments (Arkin *et al*., 1996) performed in a lipid bilayer. These cysteine SH/SD exchange experiments supported a model, described (Adams *et al*., 1995) as a result of a systematic search, which was rotated ~25° from the conformation found here (i.e. equivalent to cluster 6, see also top of Figure 5, and which is also entirely consistent with the mutagenesis data (see horizontal bars in Figure 5). This conclusion was reached as the SH groups failed to show exchange only when Cys41 was substituted by Ala. It was concluded then that Cys41 was the only cysteine residue accessible to the lipid. This interpretation, however, did not take into account a possible change in the conformation induced by mutation that would leave Cys36 and Cys46 inaccessible to exchange. This hypothetical change would not be detected by mutagenesis studies, given that the interpretation of these studies is ambiguous respect to which one of these conformations is correct. This exciting possibility is currently under study.

In addition, the systematic search (Adams *et al*., 1995) that suggested a structure equivalent to cluster 6 in Figure 5 was performed in the absence of restraints. In this respect, it is interesting to note that when we performed a simulation where β was restricted to 20°, a tilt suggested in (Adams *et al*., 1995), the cluster equivalent to cluster 5 in Figure 5 was undetected using the filters described in Materials and Methods. This could explain why a cluster equivalent to cluster 5 was not found by Adams and co-workers (Adams *et al*., 1995) and clearly underlines the importance of good experimental restraints in molecular dynamics calculations Finally, the results obtained in this work indicate that the tilt of the transmembrane segment of Plb is probably uniform and almost perpendicular to the membrane (10°). The tilt of the transmembrane helix has been investigated using FTIR (Arkin *et al*., 1995; Tatulian *et al*., 1995) using either the wild-type (i.e. the transmembrane domain and the cytoplasmic domain) or the transmembrane domain alone. According to the respective results, two models emerged, in which Plb was either a continuous helix with constant tilt, part inside and part outside the membrane (Arkin *et al*., 1995) or two helices, one inside and one outside the membrane, joined by a β-strand (Tatulian *et al*., 1995). In relation to the hydrophobic segment, the present observations support a model in which the tilt of the helices in the hydrophobic domain is small. As far as the extramembraneous part is concerned, denaturation experiments (Arkin *et al*., 1995) are inconsistent with a completely independent extramembraneous helical domain and the pure hydrophilic domain does not show α-helical conformation (Simmerman *et al*., 1989). Taking all these results into consideration, the most plausible hypothesis is that PLb is a continuous helix, forming a pentamer arranged as a leucine zipper. The accurate determination of the rotational orientation of the helices obtained here indicates that the study of changes in helical orientation due to a variety of effectors are completely feasible.

Conclusion

Plb represents an simple test case in which saturating mutagenesis and simple oligomerisation assays could not unambiguously define the correct orientation of the helices in the pentamer. In fact, the two competing models obtained are indistinguishable when comparing the sensitivity to

mutations and interaction energy per residue. Molecular dynamics simulations using spatial restraints derived from infrared site-directed dichroism have been used to determine precisely the relative orientation of these helices. This method allows acquisition and analysis of data for membrane proteins in a very short time (a few days), does not require crystallisation or huge amounts of sample and is extremely reliable.

Acknowledgements

This work was supported by a grant from the BBSRC and Wellcome to I.T.A.

References

Adams, P., Arkin, I., Engelman, D. & Brünger, A. (1995). Computational searching and mutagenesis suggest a structure for the pentameric transmembrane domain of phospholamban. *Nature Struct. Biol.* **2**, 154-162.

Arkin, I., Adams, P., MacKenzie, K., Lemmon, M., Brünger, A. & Engelman, D. (1994). Structural organization of the pentameric transmembrane alpha-helices of phospholamban, a cardiac ion chann. *EMBO J.* **13**, 4757-4764.

Arkin, I., Adams, P., Brünger, A., Smith, S. & Engelman, D. (1997). Structural perspectives of phospholamban, a helical transmembrane pentamer. *Annu. Rev. Biophys. Biomol. Struct.* **26**, 157-179.

Arkin, I., MacKenzie, K. & Brünger, A. (1997). Site-directed dichroism as a method for obtaining rotational and orientational constraints for oriented polymers. *J. Am. Chem. Soc.* **119**, 8973-8190.

Arkin, I., Mackenzie, K., Fisher, L., Aimoto, S., Engelman, D. & Smith, S. (1996). Mapping the lipid-exposed surfaces of membrane proteins. *Nature Struct. Biol.* **3**, 240-243.

Arkin, I., Rothman, M., Ludlam, C., Aimoto, S., Engelman, D., Rothschild, K. & Smith, S. (1995). Structural model of the phospholamban ion channel complex in phospholipid membranes. *J. Mol. Biol.* **248**, 824-834.

Autry, J. & Jones, L. (1997). Functional co-expression of the canine cardiac Ca^{2+} pump and phospholamban in Spodoptera frugiperda (Sf21) cells reveals new insights on ATPase regulation. *J. Biol. Chem.* **272**, 15872-15880.

Brünger, A., Adams, P., Clore, G., Gros, W., Grosse-Kunstleve, R., Jiang, J., Kuszewski, J., Nilges, M., Pannu, N., Read, R., Rice, L., Simonson, T. & Warren, G. (1998). Crystallography and NMR system: a new software system for macromolecular structure determination. *Acta Crystallog. sect. D*, **54**, 905-921.

Byler, D. & Susi, H. (1986). Examination of the secondary structure of proteins by deconvolved FTIR spectra. *Biopolymers*, **25**, 469-487.

Chu, G., Dorn, G., III, Luo, W., Hatter, J., Kadambi, V., Walsh, R. & Kranias, E. (1997). Monomeric phospholamban overexpression in transgenic mouse hearts. *Circ Res.* **81**, 485-492.

Chu, G., Li, L., Sato, Y., Harrer, J., Kadambi, V., Hoit, B., Bers, D. *et al.* (1998). Pentameric assembly of phospholamban facilitates inhibition of cardiac function *in vivo*. *J. Biol. Chem.* **273**, 33674-33680.

Cook, E., Huggins, J., Sathe, G., England, P. & Piggott, J. (1989). The expression of canine cardiac phospholamban in heterologous systems. *Biochem. J.* **264**, 533-538.

Cornea, R., Jones, L., Autry, J. & Thomas, D. (1997). Mutation and phosphorylation change the oligomeric structure of phospholamban in lipid bilayers. *Biochemistry*, **36**, 2960-2967.

Fujii, J., Maruyama, K., Tada, M. & MacLennan, D. (1989). Expression and site-specific mutagenesis of phospholamban. Studies of residues involved in phosphorylation and pentamer formation. *J. Biol. Chem.* **264**, 12950-12955.

Harrick, N. (1967). *Internal Reflection Spectroscopy*, 1st edit., Interscience publishers, New York.

Herzyk, P. & Hubbard, R. (1998). Using experimental information to produce a model of the transmembrane domain of the ion channel phospholamban. *Biophys. J.* **74**, 1203-1214.

Jorgensen, W. & Tirado-Rives, J. (1988). The OPLS potential function for proteins, energy minimization for crystals of cyclic peptides and crambin. *J. Am. Chem. Soc.* **110**, 1657-1666.

Karim, C., Stamm, J., Karim, J., Jones, L. & Thomas, D. (1998). Cysteine reactivity and oligomeric structures of phospholamban and its mutants. *Biochemistry*, **37**, 12074-12081.

Kimura, Y., Asahi, M., Kurzydlowski, K., Tada, M. & MacLennan, D. (1998). Phospholamban domain Ib mutations influence functional interactions with the Ca^{2+}-ATPase isoform of cardiac sarcoplasmic reticulum. *J. Biol. Chem.* **273**, 14238-14241.

Kimura, Y., Kurzydlowski, K., Tada, M. & MacLennan, D. (1996). Phospholamban regulates the Ca^{2+}-ATPase through intramembrane interactions. *J. Biol. Chem.* **271**, 21726-21731.

Kimura, Y., Kurzydlowski, K., Tada, M. & MacLennan, D. (1997). Phospholamban inhibitory function is activated by depolymerization. *J. Biol. Chem.* **272**, 15061-15064.

Kirchberger, M. & Tada, M. (1976). Effects of adenosine 3′,5′-monophosphate dependent protein kinase on sarcoplasmic reticulum oslated from cardiac and slow and fast contracting skeletal muscles. *J. Biol. Chem.* **251**, 725-729.

Kovacs, R., Nelson, M., Simmerman, H. & Jones, L. (1988). Phospholamban forms Ca^{2+}-selective channels in lipid bilayers. *J. Biol. Chem.* **263**, 18364-18368.

Kukol, A., Adams, P., Rice, L., Brünger, A. & Arkin, I. (1999). Experimentally based orientational refinement of membrane proteins: A structure for the influenza A M2 H^+ channel. *J. Mol. Biol.* **286**, 951-962.

Simmerman, H. & Jones, L. (1998). Phospholamban: protein structure, mechanism of action, and role in cardiac function. *Physiol. Rev.* **78**, 921-947.

Simmerman, H., Kobayashi, Y., Autry, J. & Jones, L. (1996). A leucine zipper stabilizes the pentameric membrane domain of phospholamban and forms a coiled-coil pore structure. *J. Biol. Chem.* **271**, 5941-5946.

Simmerman, H., Lovelace, D. & Jones, L. (1989). Secondary structure of detergent-solubilized phospholamban, a phosphorylatable, oligomeric protein of cardiac sarcoplasmic reticulum. *Biochim. Biophys. Acta*, **997**, 332-329.

Tatulian, S., Jones, L., Reddy, L., Stokes, D. & Tamm, L. (1995). Secondary structure and orientation of phospholamban reconstituted in supported bilayers from polarized attenuated total reflection FTIR spectroscopy. *Biochemistry,* **34**, 4448-4456.

Toyofuku, T., Kurzydlowski, K., Tada, M. & MacLennan, D. (1994). Amino acids Glu2 to Ile18 in the cytoplasmic domain of phospholamban are essential for functional association with the Ca^{2+}-ATPase of sarcoplasmic reticulum. *J. Biol. Chem.* **269**, 3088-3094.

Tsuboi, M. (1962). Infrared dichroism and molecular conformation of α-form poly-γ-benzyl-L-glutamate. *J. Polym. Sci.* **59**, 139-153.

Wegener, A. & Jones, L. (1984). Phosphorylation-induced mobility shift in phospholamban in sodium dodecyl sulfate-polyacrylamide gels. Evidence for a protein structure consisting of multiple identical phosphorylatable subunits. *J. Biol. Chem.* **259**, 1834-1841.

Wellings, D. & Atherton, E. (1997). Standard FMOC protocols. *Methods Enzymol.* **289**, 44-67.

Edited by G. von Heijne

(Received 29 March 2000; received in revised form 15 May 2000; accepted 17 May 2000)